Journal of Biomolecular NMR, **22:** 65–81, 2002.
KLUWER/ESCOM

A novel PH-CT-COSY methodology for measuring J_{PH} coupling constants in unlabeled nucleic acids. Application to HIV-2 TAR RNA

Teresa Carlomagno**, Mirko Hennig & James R. Williamson*
The Scripps Research Institute, Department of Molecular Biology and the Skaggs Institute for Chemical Biology, 10550 North Torrey Pines Rd., La Jolla, CA 92037, U.S.A.

Received 15 October 2001; Accepted 8 November 2001

Key words: constant time COSY, dipolar couplings, J_{PH} couplings, nucleic acids, phosphodiester backbone, relaxation effects

Abstract

A quantitative analysis of J_{PH} scalar couplings in nucleic acids is difficult due to small couplings to phosphorus, the extreme overlap of the sugar protons and the fast relaxation of the spins involved in the magnetization transfer. Here we present a new methodology that relies on heteronuclear Constant Time Correlation Spectroscopy (CT-COSY). The three vicinal $^3J_{PH3'}$, $^3J_{PH5'}$ and $^3J_{PH5''}$ scalar couplings can be obtained by monitoring the intensity decay of the P_i-$H3'_{i-1}$ peak as a function of the constant time T in a 2D correlation map. The advantage of the new method resides in the possibility of measuring the two $^3J_{PH5'}$ and $^3J_{PH5''}$ scalar couplings even in the presence of overlapped H5′/H5″ resonances, since the quantitative information is extracted from the intensity decay of the P-H3′ peak. Moreover, the relaxation of the H3′ proton is considerably slower than that of the H5′/H5″ geminal protons and the commonly populated conformations of the phosphate backbone are associated with large $^3J_{PH3'}$ couplings and relatively small $^3J_{PH5'/H5''}$. These two facts lead to optimal signal-to-noise ratio for the P-H3′ correlation compared to the P-H5′/H5″ correlation.
The heteronuclear CT-COSY experiment is suitable for oligonucleotides in the 10–15 kDa molecular mass range and has been applied to the 30mer HIV-2 TAR RNA. The methodology presented here can be used to measure P-H dipolar couplings (D_{PH}) as well. We will present qualitative results for the measurement of P-H_{base} and P-H2′ dipolar couplings in the HIV-2 TAR RNA and will discuss the reasons that so far precluded the quantification of the D_{PH}s for the 30mer RNA.

Abbreviations: HETCOR, HETeronuclear CORrelation; J-HMBC, J-Heteronuclear Multiple Bond Correlation; COSY, COrrelation SpectroscopY; P-FIDS (Fitting of Doublets from Singlets)-HSQC, Heteronuclear Single Quantum Coherence; HIV, Human Immunodeficiency Virus; CSA, Chemical Shift Anisotropy.

Introduction

In structural studies of nucleic acids by NMR the conformation of the phosphate backbone is often poorly defined, due to the paucity of NOE restraints. The backbone dihedral angles β, γ, δ and ε are accessible through homonuclear and heteronuclear coupling constants J_{HH}, J_{PH}, J_{CP} and J_{CH} in oligonucleotides (Schwalbe et al., 1993, 1994; Richter et al., 1998; Marino et al., 1996; Hines et al., 1993; Sklenar and Bax, 1987; Gotfredsen et al., 2001; Clore et al., 1998; Hu et al., 1999; Szypersky et al., 1997; Legault et al., 1995; Wu and Bax, 2001). However, the determination of $^3J_{PH}$ couplings particularly in RNA remains an experimentally challenging problem. HETCOR and J-HMBC techniques applied to RNA are complicated by severe spectral overlap and by the presence of competing $^3J_{HH}$ homonuclear couplings, since the H2′, H3′,

*To whom correspondence should be addressed. E-mail: jrwill@scripps.edu
**Present address: MPI for Biophysical Chemistry, Am Fassberg 11, D-37077 Goettingen, Germany, E-mail: tcarlom@gewdg.de

H4′, H5′ and H5″ ribose protons are specially overlapped and cannot be selectively inverted. E.COSY techniques are not practical, due to the lack of a well resolved passive coupling to the phosphorus. Quantitative homonuclear J-correlation spectroscopy is suitable for DNA molecules only, where the H2′/H2″ resonances are well resolved from other sugar proton resonances. In the P-FIDS-HSQC method the accuracy of the measured coupling constants diminishes substantially when $J * T_2^* < 0.15$ (Schwalbe et al., 1993), which is likely to apply to H5′/H5″ protons in RNA molecules $\geq$ 10 kDa.

Here we introduce a new methodology to measure $^3J_{PH}$ scalar couplings in RNA based on PH-CT-COSY correlation spectroscopy. The scalar couplings are obtained from the intensity modulation of cross-peaks for different constant times, similarly to existing methodologies for the measurement of H-H dipolar and scalar couplings (Billeter et al., 1992; Tian et al., 1999; Wu and Bax, 2001). The new method can be applied to unlabeled RNAs as large as 10–15 kDa. The ribose H3′ resonances are resolved by correlation to the phosphorus chemical shift. The three vicinal $^3J_{PH3'}$, $^3J_{PH5'}$ and $^3J_{PH5''}$ scalar couplings can be obtained by analyzing intensities of the P-H3′ correlation alone, that contain information on both the active $^3J_{PH3'}$ coupling and the two passive $^3J_{PH5'}$ and $^3J_{PH5''}$ couplings. In this way the problem of the extreme overlap of the geminal H5′/H5″ protons is circumvented. Moreover, the presence of conformational averaging can be effectively detected by fitting the data to different models. Effects due to coherence relaxation processes are quantitatively discussed in the Data Analysis section.

The trans activation response element TAR RNA binds to an arginine-rich region in the N-terminal domain of the Tat regulatory protein in HIV-1 and HIV-2, this event is essential for effective viral replication. The amide derivative of arginine also binds specifically to TAR, although with lower affinity (Tao et al., 1992, 1993). NMR structures of the TAR RNA both bound to argininamide and free in solution are available (Puglisi et al., 1992; Brodsky et al., 1997; Aboul-ela et al., 1996; Long and Crothers, 1999). The nucleotides important for Tat binding are clustered around a bulge (Figure 2b) and involve the bulge nucleotide U23 and the G26-C39 and A27-U38 base pairs in the upper stem region. In the free TAR RNA, the upper and lower stems have been found to be at an angle of about 50° with respect to each other (Zacharias and Hagerman, 1995). Upon binding of cognate peptides or argininamide, the bulge region undergoes a major conformational change resulting in coaxial stacking of the upper and lower stem regions and this process is likely to be accompanied by variations in the RNA backbone torsion angles. Tracking the difference in the backbone conformation between the free and bound form of the HIV-2 TAR RNA is a demanding task due to the paucity of experimental restraints. Consequently, J_{PH} scalar couplings have a major impact on the precision of the description of the backbone conformation in NMR studies. The new experiment described here will allow us to derive quantitative $^3J_{PH}$ coupling restraints that will help in defining the different phosphate backbone conformations around the torsion angles β and ε in the bound and free form of the TAR RNA. For this methodological study the 30mer HIV-2 TAR RNA was used in its unbound form.

Additionally, we have observed P-H dipolar couplings (D_{PH}) in oriented samples with the new methodology. Due to the fast phosphorus transversal relaxation and to the small size of the D_{PH}s we were unable to reliably quantify the dipolar couplings. However, qualitative results were obtained for both the P-H_{base} and P-H2′ dipolar couplings. A more accurate analysis of the D_{PH}s could be performed at lower field, where the Chemical Shift Anisotropy contribution to the phosphorus transversal relaxation is remarkably reduced.

Methodology

Pulse sequence

To measure $^3J_{PH}$ coupling constants we propose to use the PH-CT-COSY pulse sequence, shown in Figure 1a, that represents a Constant Time (CT) version of the PH-COSY experiment proposed by Sklenar (Sklenar et al., 1986). After saturating the protons with a series of 120° pulses separated by 5 ms delays for about 3 s, transverse phosphorus magnetization is generated by the first 90°(P) pulse. During the constant time T, magnetization evolves under the effect of $^3J_{PH}$ scalar couplings and the term $2P_xH_z$, present at point b, is transformed in the observable $2H_yP_z$ term by the last two 90°(P) and 90°(H) pulses. The observed signal is dispersive and antiphase with respect to the $^3J_{PH}$ coupling.

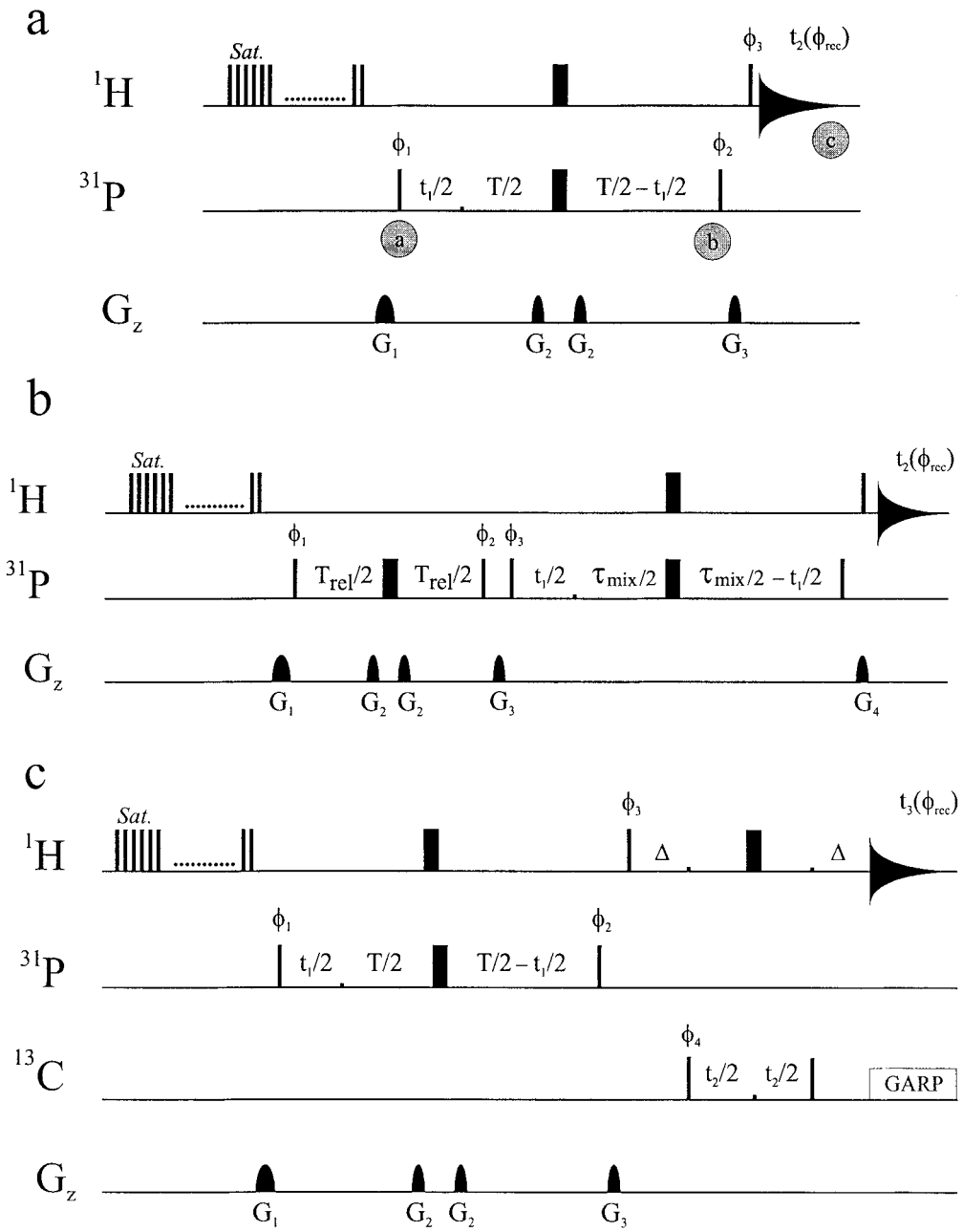

Figure 1. (a) PH-CT-COSY sequence. The brief product operator description at time points a, b and c is given in the text. The protons were saturated with a series of 120° pulses for 3 s with an RF field of 28 kHz. The phases are: $\phi_1 = 0, 2$; $\phi_2 = 1, 1, 3, 3$; $\phi_3 = 0, 0, 0, 0, 2, 2, 2, 2$; $\phi_{rec} = 0, 2, 2, 0, 2, 0, 0, 2$. The pulses without explicit phase settings are applied along x. The constant time T was varied between 20 and 80 ms. (b) Sequence for the measurement of R_2^*. The phases are: $\phi_1 = 0, 2$; $\phi_2 = 0, 0, 2, 2$; $\phi_3 = 1, 1, 1, 1, 3, 3, 3, 3$; $\phi_{rec} = 0, 2, 2, 0, 2, 0, 0, 2$. τ_{mix} was equal to 40 ms and T_{rel} was varied between 1 and 70 ms. (c) Similar to (a) with a ^{13}C-^{1}H HMQC editing step added at the end of the pulse sequence. $\Delta = 3.4$ ms. Quadrature detection in the phosphorus and carbon dimensions was obtained by altering ϕ_1 and ϕ_4, respectively, according to States-TPPI.

The product operator description of the sequence at points a, b and c (Figure 1a) is as follows:

(a) $-P_y$,
(b) $2P_xH_{lz}\sin(\pi J_{H_lP}T)\Pi_k\cos(\pi J_{H_kP}T)\exp(-R_2^*T)$,
(c) $2P_zH_{ly}\sin(\pi J_{H_lP}T)\Pi_k\cos(\pi J_{H_kP}T)\exp(-R_2^*T)$,

where H_l is the nucleus observed in t_2 and H_k are the protons passively coupled to the phosphorus. R_2^* is the effective relaxation rate of the transverse phosphorus magnetization that includes contributions from the phosphorus R_2 and the R_1 of the protons scalar coupled to the phosphorus. In the following analysis, we make the assumption that the effective relaxation rate R_2^* during the constant time can be measured by monitoring the decay of the magnetization with increasing the relaxation delay T_{rel} (Figure 1b). In this PH correlation, magnetization is transferred from the phosphorus to the proton during the time τ_{mix}, as in the PH-CT-COSY sequence described above. However, during the relaxation delay T_{rel}, the transverse magnetization of phosphorus nuclei relaxes with an effective relaxation constant which is equal to R_2^*, provided that the following two assumptions are fulfilled: (a) $(2\pi J_{PHl})^2 > (R_P\text{-}R_{PH})^2$ (Cavanagh et al., 1996), where R_P is the R_2 relaxation rate of the phosphorus nucleus and R_{PH} is the relaxation rate of the antiphase term $2P_xH_{lz}$; (b) potentially contributing cross-correlated relaxation rates, such as $\Gamma_{P,PH}$ between the ^{31}P-CSA and the ^{31}P-^{1}H3′ dipolar interactions, are small enough to be neglected. The first assumption is obviously not always fulfilled especially for the H5′/H5″ protons, due to the fast R_1 of the geminal H5′/H5″ protons and to the small $^3J_{PH5'/H5''}$ coupling constants in a standard A-form helix. We will provide evidence based on theoretical simulations that this does not bias the accuracy of the measured $^3J_{PH}$ scalar couplings. This observation is due to the fact that the most efficient mechanism of magnetization transfer during each half of the T or T_{rel} delays in the experiments of Figures 1a and 1b is the scalar coupling to the H3′ proton. The H3′ proton also has the longest T_1 and the condition $(2\pi J_{PH})^2 \gg (R_P\text{-}R_{PH})^2$ is fulfilled for the P-H3′ spin system in the 30mer RNA used in the present study, which approximates the condition $(2\pi J_{PHl})^2 \gg (R_P\text{-}R_{PH})^2$. The value of the $\Gamma_{P,PH}$ cross-correlated relaxation depends on the global correlation time τ_c and the projection angle between the P-H3′ distance vector and the directions of two of the principal axis of the phosphorus CSA tensor. Assuming a τ_c of 4.0 ns (unpublished results) at 298 K for the 30mer RNA used in this work and CSA tensor components according to Herzfeld et al. 1984), the maximum possible value of the $\Gamma_{P,PH}$ is 6.0 Hz. However, theoretical simulations verified that the difference in the R_2^* values measured using the sequence of Figure 1b for a J-coupled (P, H3′, H5′, H5″) four-spin system with cross-correlated relaxation rates $\Gamma_{P,PH3'}$ of 6.0 Hz and 0.0 Hz is only 2%, which is well within the experimental error. The $\Gamma_{P,PH}$ does not contribute to the magnetization transfer pathway in the experiment of Figure 1a, due to the presence of the π(H) pulse in the middle of the constant time T.

The two-dimensional P-H correlation of a 1.5 mM isotropic solution of the 30mer HIV-2 TAR RNA in D_2O is shown in Figure 2a, together with a schematic representation of the secondary structure of the RNA (Figure 2b). The spectrum was obtained with the pulse sequence of Figure 1a. Due to the partial overlap of the H3′ and H5′/H5″ resonances, only 58% of the signals can be quantitatively analyzed. Resolved spectra can be obtained by adding a ^{13}C editing step to the experiment of Figure 1a, as outlined in Figure 1c (Varani et al., 1995). In Figure 3 the ^{13}C-^{1}H plane corresponding to the phosphorus resonance of A22 and C46 at −4.01 ppm is shown: the two P_{22}-($C3'_{21}$)-$H3'_{21}$ and P_{46}-($C3'_{45}$)-$H3'_{45}$ peaks, that overlap in the P-H 2D map of Figure 2a, are well resolved. Alternatively, for unlabeled RNAs an additional proton editing step through a NOESY correlation with the well resolved H1′ protons could be used as well.

Data analysis

Ten experiments with constant time duration T spanning the range 18–82 ms were recorded for the HIV-2 TAR RNA on a Varian INOVA 600 MHz spectrometer using the pulse sequence of Figure 1a. In order to discuss the procedure used to extract coupling constants and the effect of relaxation processes on the accuracy of the results, we will focus on the peaks corresponding to the correlations between the phosphorus of U40 and U31 and the H3′ proton of the preceding nucleotide. The R_2^* relaxation rates for U40 and U31, measured with the experiment of Figure 1b by fitting the decay of the signal intensity as a function of T_{rel} to a mono-exponential decay function, are 35.0 ± 0.7 Hz and 27.7 ± 0.5 Hz, respectively. The signal decay with increasing constant time T values, measured with the experiment of Figure 1a for the connectivity P_{40}-$H3'_{39}$, is shown in Figure 4a. The signal intensity can be described by the function:

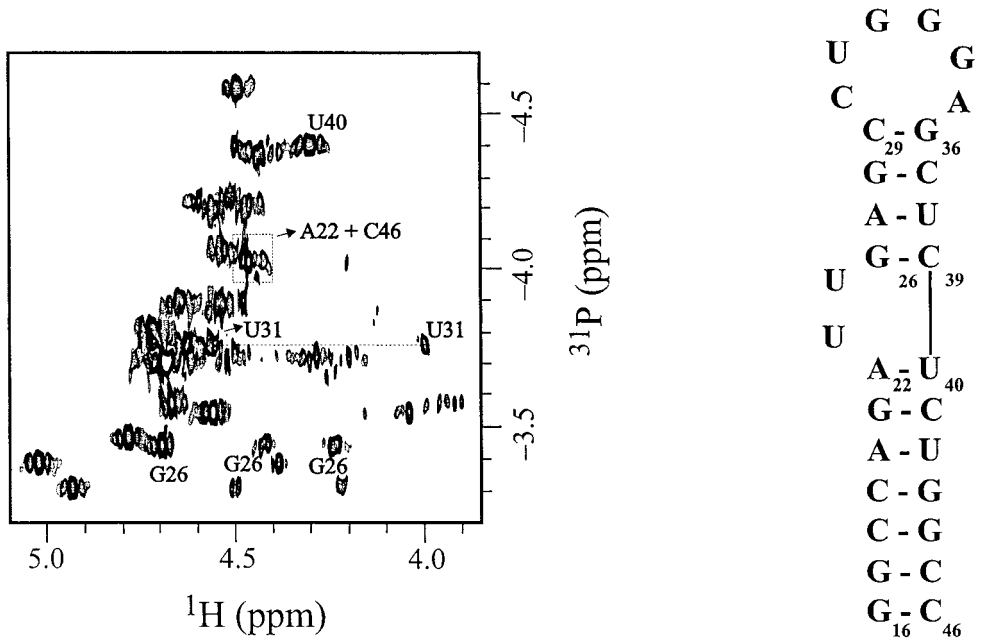

Figure 2. (a) Two-dimensional P-H correlation recorded with the sequence of Figure 1a for the 30mer HIV-2 TAR RNA, showing P-H3′ and P-H5′/H5″ cross peaks. The proton carrier was at 4.78 ppm and the phosphorus carrier was at −3.65 ppm. Sixteen complex points were acquired for the phosphorus dimension. After mirror image linear prediction in the indirect dimension and zero-filling in both dimensions, the final matrix was 2048(ω_2) × 128(ω_1) points. The constant time T was 40 ms for the spectrum shown here. All spectra were recorded on a four-channel Varian Inova 600 MHz spectrometer equipped with an actively shielded z-gradient triple resonance probe, at a temperature of 298 K. Spectra were processed and analyzed with FELIX 2000 (MSI, San Diego, U.S.A.). The sample buffer contained 10 mM phosphate buffer, pH 6.4, 50 mM sodium chloride, and 0.1 mM EDTA in 500 µl of 99.9% D_2O. (b) Secondary structure of the 30mer HIV-2 TAR RNA.

$$I_R(T) = I_0 \exp(-R_2^* T) \sin(\pi J_{PH3'} T) \cos(\pi J_{PH5'} T) \cos(\pi J_{PH5''} T) \Sigma_k \cos(\pi J_{PHk} T) \quad (1)$$

where J_{PHk} represents passive P-H couplings other than the $^3J_{PH5'/H5''}$, such as the long-range $^4J_{PiH4'i}$ and the $^4J_{Pi,H2'i-1}$. After deconvoluting the dependence of $I_R(T)$ on R_2^*, the data of Figure 4b is obtained. The time dependence of the signal intensity is now described by the function:

$$I(T) = I_0 \sin(\pi J_{PH3'} T) \cos(\pi J_{PH5'} T) \cos(\pi J_{PH5''} T) \Sigma_k \cos(\pi J_{PHk} T) \quad (2)$$

The P_{40}-$H5'_{40}$ and P_{40}-$H5''_{40}$ correlations are not observable due to low signal-to-noise ratio. However, we will show that the time dependence of the intensity of the single J-mediated cross peak P_{40}-$H3'_{39}$ is sufficient to reveal the presence of the two additional passive coupling partners to the P_{40} nucleus, namely the H5′ and H5″ protons. In a first approximation and for the sake of simplicity we will assume that the $^4J_{PiH4'i}$ and $^4J_{Pi,H2'i-1}$ are close to zero and will neglect them. The presence of these additional passive long-range couplings and their effect on the accuracy of the extracted $^3J_{PH3'}$ and β angle will be discussed at the end of this section.

Erroneously assuming, from the observation of one P-H peak only, that the P_{40} nucleus has a single proton coupling partner, we would try to fit the data of Figure 4b to the function:

$$I(T) = I_0 \sin(\pi J_{PH3'} T) \quad (3)$$

(gray curve), obtaining very poor agreement between the experimental and the simulated data. The parameter set of the fitting procedure comprises the intensity I_0 and the coupling constant $^3J_{PH3'}$. A remarkably better fitting of the experimental data is obtained using the function of Equation 2 (black line), which describes the cross-peak intensities as dependent on both the

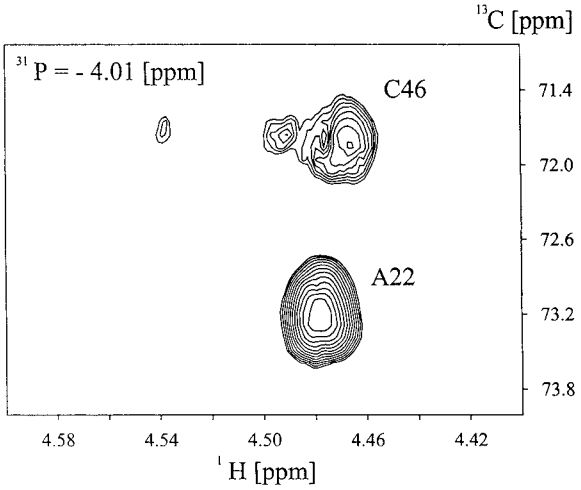

Figure 3. ^{13}C-^{1}H plane for the P-C-H correlation acquired with the sequence of Figure 1c. The two peaks corresponding to the P_{22}-($C3'_{21}$)-$H3'_{21}$ and P_{46}-($C3'_{45}$)-$H3'_{45}$ correlations, that are overlapped in the spectrum of Figure 2a, are well resolved here in the ^{13}C dimension. Twelve and forty-eight complex points were acquired for the phosphorus (t_2) and the carbon (t_1) dimensions, respectively; after linear prediction in the indirect dimensions and zero-filling in all dimensions, the final matrix was 2048(ω_3) × 128(ω_2) × 256(ω_1) points. The constant time T was 37 ms.

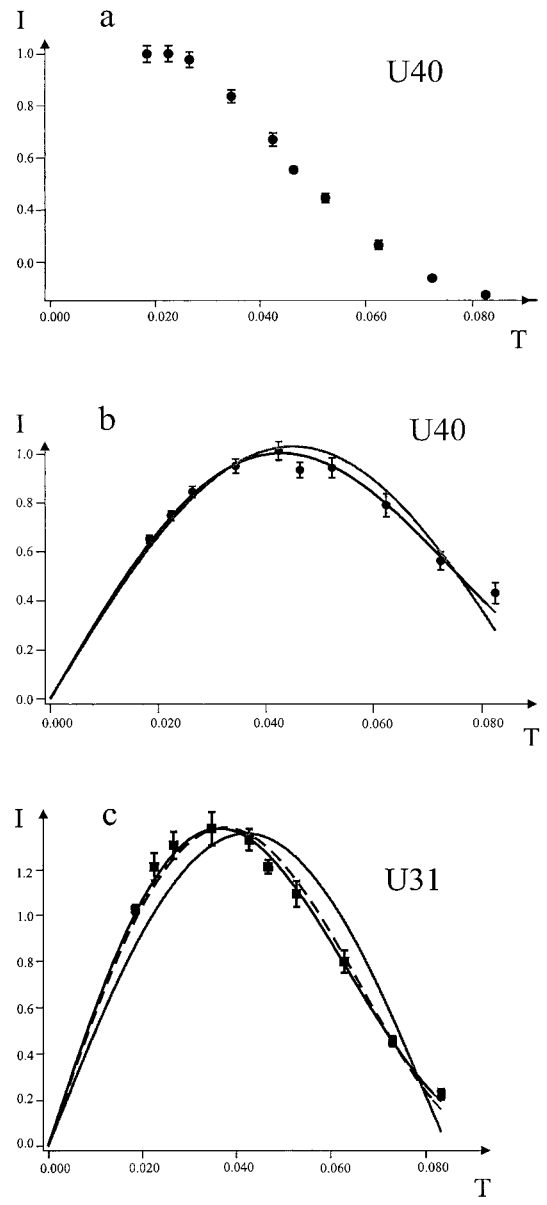

Figure 4. (a) Decay of the signal intensity as a function of the constant time T for the peak P_{40}-$H3'_{39}$ in the experiment of Figure 1a. T was varied between 18 and 82 ms. (b) Data points of Figure 4a after multiplication by exp(R_2^*T) with $R_2^* = 35.0 \pm 0.7$. The gray and black curves correspond to fitting the data to the function of Equation 3 and 2, respectively. A decrease of the χ^2 value from 31 to 8 and a large F-statistics value ($19 > F_{0.05} = 5.6$) indicate that the data is appropriately described by the function of Equation 2, leading to $^3J_{PH3'} = 9.2 \pm 0.6$ Hz, $\beta = 168/192° \pm 2.0$. (c) The data are of the same kind of (b) for the peak P_{31}-$H3'_{30}$. The gray curve corresponds to data fit applying Equation 3, the dashed black curve represents the fitting of the data to Equation 2, with $^3J_{PH5'}$ and $^3J_{PH5''}$ following a Karplus dependence on β, and the continuous black curve represents the fitting of the data to Equation 2 assuming $^3J_{PH5'} = {}^3J_{PH5''}$. The χ^2 value decreases from 24 to 7 when fitting the data to Equation 2 assuming $^3J_{PH5'} = {}^3J_{PH5''}$ (continuous black line) compared to $^3J_{PH5'} \neq {}^3J_{PH5''}$ (dashed black line), indicating conformational averaging around the β torsion angle.

active coupling $^3J_{PH3'}$ and the two passive couplings $^3J_{PH5'/5''}$ ($^4J_{PHk} = 0.0$ Hz). The two $^3J_{PH5'/5''}$ scalar couplings are not fitted independently: it is assumed that they follow the parameterized Karplus dependence on the torsion angle β (Figure 5a) (Lankhorst et al., 1984). The parameter set of the fitting procedure comprises the intensity I_0, the coupling constant $^3J_{PH3'}$ and the torsion angle β (the best fit is obtained for $^3J_{PH3'} = 9.2 \pm 0.6$ Hz, $\beta = 168/192° \pm 2°$. The introduction of the additional fitting parameter β is justified by a high F-statistics value. This result verifies that the coupling constant $^3J_{PH3'}$ and the torsion angle β can be efficiently measured by analyzing the time dependence of the P_i-$H3'_{i-1}$ peak alone, with considerably better signal-to-noise ratio and resolution compared to the P_i-H5′/$H5''_i$ correlation. It shall be noted that the high precision obtained on the angle β reflects the fact that the two passive $^3J_{PH5'/H5''}$ are not independent of each other. Any β value significantly deviating from 180° would give rise to at least one large (> 6.0 Hz) $^3J_{PH5'/H5''}$, which would be clearly detectable in the time-dependence of the P-H3′ peak intensity. Thus, the applied fitting procedure detects the absence of such a high passive coupling (160° < β < 200°) and, due to the correlation of the two $^3J_{PH5'/H5''}$, returns a very precise β value. However, because of internal

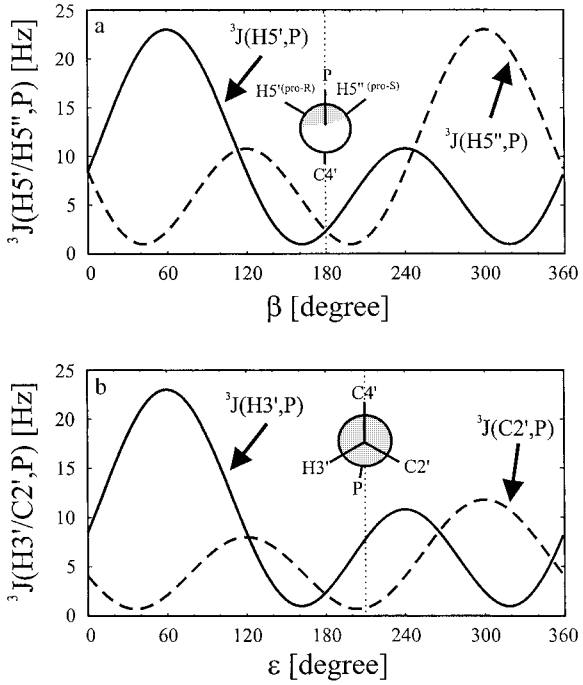

Figure 5. Karplus dependence of the $^3J_{PH5'}$ and $^3J_{PH5''}$ couplings on the torsion angle β (panel a) and of the $^3J_{PH3'}$ and $^3J_{PC2'}$ scalar coupling on the torsion angle ε (panel b), according to the equation $^3J_{PH} = 15.3\cos^2\theta - 6.1\cos\theta + 1.6$ and $^3J_{PC} = 9.1\cos^2\theta - 1.9\cos\theta + 0.8$ (Lankhorst et al., 1984; Plavec and Chattopadhyaya, 1995).

fluctuations, this result has to be considered as an average value and a larger tolerance than the reported error Δβ should be allowed for β in structure calculations.

The nucleotide U31, located at the beginning of the hexanucleotide loop, exhibits conformational averaging around the β torsion angle, as can be concluded from the degenerate chemical shifts of the geminal H5′/H5″ protons. In this case the data can be optimally fitted to the function of Equation 2, imposing $^3J_{PH5'} = {}^3J_{PH5''}$ (continuous black line, Figure 4c) ($^3J_{PH3'} = 9.5 \pm 0.6$ Hz; $^3J_{PH5'} = {}^3J_{PH5'} = 4.5 \pm 0.2$ Hz). Assuming a Karplus dependence of the $^3J_{PH5'}$ and $^3J_{PH5''}$ on a single β rotamer (dashed black line) leads to an unsatisfactory fitting of the experimental data, according to the χ^2 test. The χ^2 and F-statistic values for the data fitting of the connectivities P_{40}-$H3'_{39}$ and P_{31}-$H3'_{30}$ are given in the caption to Figure 4. The resulting $^3J_{PH3'}$ and β values for 16 of the 29 HIV-2 TAR RNA nucleotides are summarized in Table 1 (columns 2 and 6). Interestingly, a remarkable amount of valuable information can be derived from the time dependence of the intensity of one single cross peak, which makes this method superior to any spin echo based quantitative J correlation scheme in its ability to unravel additional coupling partners and detect conformational averaging.

Up to this point we have assumed that the additional passive $^4J_{PiH4'i}$ and $^4J_{Pi,H2'i-1}$ coupling constants are close to zero. However, the $^4J_{PH}$ coupling can reach values as high as 2.5–3.0 Hz when the four intervening bonds are coplanar and describe a W shape (Wijmenga and van Buuren, 1998). This is the case for the $^4J_{PiH4'i}$ in standard B-form helical geometry ($\gamma = 36°$ and $\beta = 213°$) and in DNA molecules this coupling often gives rise to an observable P_i-$H4'_i$ peak in a P-H correlation map. However in the A-form helical geometry the W shape is distorted ($\gamma = 54°$ and $\beta = 178°$ and the $^4J_{PiH4'i}$ couplings are expected to be smaller than 2.5–3.0 Hz. To verify this, we measured the $^4J_{PiH4'i}$ couplings in a spin-echo difference experiment (Hu et al., 1999) for the HIV-2 TAR RNA. Despite the extensive overlap of the C4′-H4′ correlation in helical regions, the absence of significant intensity difference between the reference and attenuated spectra allows us to conclude that the $^4J_{PiH4'i}$ coupling constants are smaller than 1.8 Hz in helical regions (1.8 Hz represents the smallest coupling constant value that would give rise to an observable intensity difference, given the S/N ratio and the constant time length in the experiment). Only five nucleotides, located in non-regular structural regions, show $^4J_{PiH4'i}$ coupling constants larger than 1.8 Hz, namely U23 (2.8 ± 0.3 Hz), C30 (2.4 ± 0.3 Hz), C31 (2.5 ± 0.3 Hz), G32 (1.8 ± 0.4 Hz) and the terminal nucleotide C46 (3.3 ± 0.3 Hz). In the P-H correlation map of the HIV-2 TAR RNA we do not observe any P_i-$H4'_i$ peak. Despite these observations, we repeated the fitting of the experimental data to Equation 2, assuming $^4J_{PiHi} \neq 0$. The $^4J_{PiH4'i}$ is included in the parameters set of the fitting procedure and is varied between 0.1 and 2.9 Hz. The optimal $^3J_{PH3'}$ and β values obtained are reported in the columns 3 and 7 of Table 1. The F-statistics test for introducing a new parameter in the fitting procedure ($F_{0.1}$) is negative for all data sets. This result verifies that no information on the magnitude of the additional small $^4J_{PiH4'i}$ coupling is contained in our data, due to the limited time-domain sampled. Therefore the $^4J_{PiH4'i}$ coupling cannot be reliably determined with the methodology presented here. However, the $^3J_{PH3'}$ and β values obtained from fitting the experimental data to Equation 2 using $^4J_{PiH4'i} = 0$ Hz and allowing $0.1 \leq {}^4J_{PiH4'i} \leq 2.9$ Hz are virtually the same, con-

Table 1.

Nucleotide number	$^3J_{PiH3'i-1}$ (Hz) without $^4J_{PiH4'i}$	$^3J_{PiH3'i-1}$ (Hz) with $^4J_{PiH4'i}$	$^3J_{PiH3'i-1}$ (Hz) from a spin-echo difference method	$^3J_{PiC2'i-1}$ (Hz)	β (°) or average $^3J_{PiH5'i}$ (Hz) without $^4J_{PiH4'i}$	β (°) or average $^3J_{PiH5'i}$ (Hz) with $^4J_{PiH4'i}$	$^3J_{PiH5'/5''i}$ (Hz) from a spin-echo difference method	$^4J_{PiH4'i}$ (Hz)
G17	9.6 ± 0.9	9.2 ± 1.2	8.8 ± 0.4	1.0 ± 1.0	168/192 ± 4	172/188 ± 7	–	2.0 ± 0.9
A20	7.1 ± 1.7	6.4 ± 2.2	–	–	173/187 ± 7	173/187 ± 7	–	1.5 ± 1.4
G26	14.2 ± 0.1	13.8 ± 0.2	8.6 ± 0.2	3.5 ± 0.4	156/204 ± 1	156/204 ± 1	–	2.6 ± 0.3
C29	9.1 ± 0.6	8.4 ± 0.3	8.5 ± 0.8	0.6 ± 0.6	169/191 ± 3	170/190 ± 3	–	2.7 ± 0.2
C30	8.5 ± 1.4	7.9 ± 1.8	–	0.7 ± 0.7	172/188 ± 7	173/187 ± 7	–	1.5 ± 1.4
U31	9.5 ± 0.6	9.5 ± 0.5	8.5 ± 0.7	–	4.5 ± 0.2	4.2 ± 0.2	5.2 ± 0.2	2.6 ± 0.3
G32	8.8 ± 0.6	8.7 ± 0.5	8.2 ± 0.2	–	4.2 ± 0.2	3.9 ± 0.2	4.6 ± 0.2	2.4 ± 0.5
A35	9.5 ± 0.5	9.3 ± 0.4	9.0 ± 0.6	5.4 ± 0.2	4.6 ± 0.2	4.4 ± 0.2	4.9 ± 0.2	2.6 ± 0.3
G36	11.0 ± 0.3	10.8 ± 0.1	8.3 ± 0.6	3.8 ± 0.3	162/198 ± 1	164/196 ± 1	–	2.8 ± 0.1
C37	9.3 ± 1.3	8.8 ± 1.5	8.7 ± 0.5	2.5 ± 0.5	169/191 ± 6	172/188 ± 8	–	1.4 ± 1.3
U38	6.5 ± 3.0	undetermined	–	–	172/188 ± 8	172/188 ± 8	–	1.5 ± 1.4
C39	9.2 ± 0.9	8.6 ± 1.0	8.1 ± 1.2	–	169/191 ± 4	173/187 ± 7	–	1.8 ± 1.1
U40	9.2 ± 0.6	8.7 ± 0.6	9.6 ± 0.9	–	168/192 ± 2	168/192 ± 2	–	2.5 ± 0.4
C41	8.8 ± 1.6	8.5 ± 1.6	–	–	172/188 ± 8	172/188 ± 8	–	1.5 ± 1.4
G44	9.2 ± 0.5	8.7 ± 0.6	9.4 ± 0.2	1.7 ± 0.6	169/191 ± 2	170/190 ± 3	–	2.6 ± 0.3
C45	8.3 ± 1.2	7.7 ± 1.4	6.8 ± 0.9	0.8 ± 0.8	173/187 ± 7	174/186 ± 6	–	1.7 ± 1.2

$^3J_{PH3'}$ coupling constants and β torsion angles for the nucleotides of the HIV-2 TAR RNA listed in column 1, extracted by analysis of the data obtained with the sequence of Figure 1a, as explained in the Data analysis section. Two possible values of β satisfy the experimental data, due to the lack of stereospecific assignment of the H5′/H5″ protons. The errors on $^3J_{PH3'}$ and β represent the standard deviation of the parameters derived by fitting the experimental intensities to Equation 2. Columns 2 and 6 report on the results of fitting the experimental intensities to Equation 2 with $^4J_{PiH4'i} = 0$ (three parameters fitting: I_0, $^3J_{PH3'}$, β); columns 3 and 7 report on the results of fitting the experimental intensities to Equation 2 with $0.1 \leq {}^4J_{PiH4'i} \leq 2.9$ Hz (four parameters fitting: I_0, $^3J_{PH3'}$, β, $^4J_{PiH4'i}$).

firming that the presence of an additional small passive coupling does not bias the extraction of $^3J_{PH3'}$ and β. One exception is represented by U38: due to the large experimental uncertainties for the intensities of the peak P_{38}-$H3'_{37}$, the $^3J_{PH3'}$ value remains undetermined ($0.0 < {}^3J_{PH3'} < 10.0$ Hz) in the four parameter fitting (I_0, $^3J_{PH3'}$, β and $^4J_{PiH4'i}$).

The $^4J_{PiH2'i-1}$ coupling approaches 2.5–3.0 Hz when ε is in the *gauche-* conformation. This situation occurs for none of the measured ε torsion in the HIV-2 TAR RNA, with the possible exception of conformational averaging between the *trans* and *g-* conformations for the hexaloop nucleotides (see Results section). $^4J_{PiH2'i-1}$ couplings larger than 1.0 Hz were found for A27, G33 and G34 in a spin-echo difference experiment (Hu et al., 1999); however none of these nucleotides is included in the present study. Therefore the $^4J_{PiH2'i-1}$ passive coupling can be safely neglected in our case.

In general, the effect of an additional small passive coupling constant on the accuracy of the $^3J_{PH3'}$ and β angle values is negligible, provided that the $^3J_{PH3'}$ is large. On the other hand, if $^3J_{PH3'} \leq 2 * {}^4J^{max}_{PiH4'i}$, the potential presence of the passive $^4J_{PiH4'i}$ can affect the accuracy of the $^3J_{PH3'}$ value by as much as 50%. In such cases, additional information should be obtained on the ε torsion (e.g., $^3J_{PC2'}$ coupling constant) and the extracted $^3J_{PH3'}$ value should be considered as an upper bound for the effective $^3J_{PH3'}$.

The validity of the proposed methodology has been verified by comparing the $^3J_{PH3'}$ values obtained with the PH-CT-COSY approach with the ones derived from a spin echo difference experiment (Table 1) (Vuister et al., 1998; Clore et al., 1998; Hu et al., 1999). The agreement is excellent with the sole exception of G26 and G36. The reason for this discrepancy will be discussed in the following section. The average value of the $^3J_{PH3'}$ coupling constants in helical regions, derived from the spin-echo difference experiment, is 8.7 Hz, which is identical to the value obtained with the PH-CT-COSY methodology. The $^3J_{PH5'/H5''}$ averaged coupling constants, extracted from the spin-echo difference experiment (Hu et al., 1999), for the three residues in the hexanucleotide loop that show conformational averaging of the H5′/H5″ protons, are also in good agreement with the values derived from the PH-CT-COSY experiment. It is noted that the $^3J_{PH5'/H5''}$ coupling constants for the nucleotides that do not experience conformational averaging around the β torsion could not be measured with the spin-echo difference approach, due to low S/N ratio and extensive spectral overlap.

We have demonstrated that it is possible to derive the $^3J_{PH3'}$ coupling constant and the β torsion angle from the intensity decay of the P-H3′ peak. However, due to the highly correlated nature of the three parameters I_0, $^3J_{PH3'}$ and β in the fitting procedure, the potential benefits and limitations of this approach deserve an additional comment. If the error of the experimental intensities, after deconvolution of the relaxation term, is ≥ 10%, large uncertainties are obtained for $^3J_{PH3'}$. Similarly to what Billeter et al. found (1992), we observe that the function $\chi^2(^3J_{PH3'})$ is very steep for $J_{PH3'} > J_{PH3',min}$* but rather shallow for $^3J_{PH3'} < {}^3J_{PH3',min}$. On the other hand the χ^2 (β) function is steep on both sites of β_{min}, as discussed previously in this section. If the precision of the experimental data is low, a continuum of solutions is found for $^3J_{PH3'} < {}^3J_{PH3',min}$. However, even in such an unfavorable case, the conformational space consistent with the experimental data can be restricted. Low values of $^3J_{PH3'}$ correlate with low values of β and high values of I_0. The combinations of $^3J_{PH3'}$ and β for which one $^3J_{PH5'/5''}$ becomes larger than $^3J_{PH3'}$ can be excluded, provided that a strong P-H3′ peak and no P-H5′/H5″ peaks are observed in the spectrum. This is justified by the fact that the amount of magnetization transferred from the phosphorus to each proton nucleus depends on the relative size of the $^3J_{PH}$ couplings and if $^3J_{PH5'/5''} > {}^3J_{PH3'}$, the pattern of the P-H3′ and P-H5′/H5″ peaks should be different from what one usually observes in RNA (strong P-H3′ peak and vanishingly small P-H5′/H5″ peaks). If the uncertainty of the experimental intensities is less than 10%, the $^3J_{PH3'}$ coupling and the torsion angle β can be determined to a good degree of accuracy, as demonstrated in Table 1.

Lastly, as it is extensively discussed in the Simulations section, the accuracy of the method relies on the possibility of acquiring data points for constant time periods as long as $1/^3J_{PH3'}$. If the $^3J_{PH3'}$ is substantially smaller than $1/CT_{max}$ the accuracy of the extracted $^3J_{PH3'}$ and β torsion angle decreases. For a $^3J_{PH3'} = 4.5$ Hz and $CT_{max} = 80$ ms, the $^3J_{PH3'}$ can be determined with an accuracy of 50% and the β torsion angle with an accuracy of 8%. Thus, the presented data analysis is well suited for RNA molecules. For DNA molecules ($^3J_{PH3'} = 1.2$ Hz in standard B-form

*$J_{PH3',min}$ and β_{min} correspond to $^3J_{PH3'}$ and β at the minimum value of χ^2.

helix) the analysis could be carried out in an analogous manner on the most intense of the P-H5′/H5″ peaks, rather than on the P-H3′ peak.

Results

Seventeen spin systems out of 29 could be quantitatively analyzed for the HIV-2 TAR RNA. The P-H3′ resonances corresponding to the remaining 12 spin systems overlap with other cross peaks in the 2D P-H spectrum but can be resolved in a 3D carbon edited experiment acquired with the pulse sequence suggested in Figure 1c. The $^3J_{PH3'}$ coupling constants and β angles are reported in Table 1, for both the three parameter fitting (I_0, $^3J_{PH3'}$, β) with $^4J_{PiH4'i} = 0.0$ Hz (columns 2 and 6) and the four parameter fitting (I_0, $^3J_{PH3'}$, β and $^4J_{PiH4'i}$) with $0.1 \leq {}^4J_{PiH4'i} \leq 2.9$ Hz (columns 3 and 7). Additionally, $^3J_{PC2'}$ couplings have been measured (Szypersky et al., 1997; Legault et al., 1995) for a ^{13}C labeled HIV-2 TAR RNA to determine the torsion angle ε (Table 1).

The β and ε angle values (Table 2) for G17, A20, C29, C30, C37, U38, C39, U40, C41, G44 and C45 are in agreement with the expected values for a regular A-form helix (Saenger, 1984; Brodsky et al., 1997; Aboul-ela et al., 1996).

U31, G32 and A35, that are part of the hexanucleotide loop capping the upper stem, show fast conformational averaging around the torsion angle β, as can be concluded by the degenerate chemical shift of the H5′/H5″ protons. The data could be best fitted to the function of Equation 2 with $^3J_{PH5'} = {}^3J_{PH5''}$. The nucleotide G33, that is located in the middle of the hexanucleotide loop, shows two distinguished resonance frequencies for the H5′/H5″ protons, both around 3.95 ppm. The intensity decay of the peak P_{33}-$H3'_{32}$ could not be fitted to any of the discussed models, probably due to the presence of a more complicated averaging mechanism. The average $^3J_{PH5'/5''}$ coupling constant values for U31, G32 and A35 are consistent with fast conformational averaging of the β torsion in the range $90° < \beta < 270°$ with equal distribution probability for each β value. For A35 both $^3J_{PH3'}$ and $^3J_{PC2'}$ coupling constants are available. The two values cannot be explained assuming a single rotamer for the ε torsion. The *g*- rotamer must be partially populated in order to account for the high value of the $^3J_{PC2'}$ coupling while the rotamer with $\beta \approx 220°$ would justify the high $^3J_{PH3'}$ value. A similar situation cannot be excluded for U31 and G32, for which the $^3J_{PC2'}$ coupling constants are not available.

The $^3J_{PH3'}$ values for G26 and G36 are significantly higher than the average, and in particular the $^3J_{PH3'}$ of G26 can only be justified by assuming that the strongly disfavored *g*+ conformer for the ε torsion angle is partially populated (Murthy et al., 1999). Moreover, the $^3J_{PH3'}$ values obtained with the PH-CT-COSY methodology substantially differ from the ones derived from the spin-echo difference experiment. Being the P-H5′/H5″ connectivities of G26 and G36 observable in the PH-CT-COSY spectra, a third estimate of the $^3J_{PH3'}$ coupling can be obtained by the 'cross peak nulling method' (Wu and Bax, 2001). This approach leads to $^3J_{PH3'}$ coupling constants close to 7.0 Hz for both G26 and G36. Additionally, the intensities of the two P-H5′ and P-H5″ peaks of G26 are quite similar, in contrast to what one would expect for a β angle of 156° ($^3J_{PH5'/5''} = 6.7$ Hz and 1.1 Hz). Lastly, the $^3J_{PH3'}$ and the $^3J_{PC2'}$ coupling constants of G26 are not consistent with the presence of a single rotamer for the ε torsion. The discrepancies found for the coupling constants of these two nucleotides can be explained by assuming slow conformational exchange. If the conformational exchange is in the milliseconds time-scale or slower, partial or no averaging of the coupling constants is obtained during the constant time period. In this case the values of the $^3J_{PH3'}$ and $^3J_{PH5'/5''}$ depend on both the length of the constant time and the nature of the dependency of the peak intensities on the couplings (e.g. sine function in the PH-CT-COSY approach and cosine function in the spin-echo difference approach). In support to this explanation, two slightly different phosphorus and proton chemical shifts are observable for each of the P-H5′ and P-H5″ correlations of G26 (Figure 2). Although both the $^3J_{PH3'}$ and the $^3J_{PC2'}$ coupling constants of G36 are consistent with $\varepsilon = 239°$, the dependence of the $^3J_{PH3'}$ on the measurement method, the similarity of the coupling constants values with those of G26, and the fact that the phosphate group of G36, like the phosphate group of G26, is situated at the 3′ end of a non-regularly structured region strongly suggest that both nucleotides experience a similar conformational exchange.

Finally, we have also applied the PH-CT-COSY methodology to a 14mer RNA comprising a stem region and the conserved GAAG tetraloop that caps helix23a of the 16S rRNA in all eu-bacteria (data not shown). The experimental uncertainties on the intensities data for this molecule are notably smaller

Table 2.

Nucleotide number	ε (°) without $^4J_{PiH4'i}$	ε (°) with $^4J_{PiH4'i}$	β (°) or average $^3J_{PiH5'i}$ (Hz) without $^4J_{PiH4'i}$	β (°) or average $^3J_{PiH5'i}$ (Hz) with $^4J_{PiH4'i}$
A-form helical regions				
G17	220 ± 6	218 ± 8	168/192 ± 4	172/188 ± 7
A20	*206* ± 10	*203* ± 12	173/187 ± 7	173/187 ± 7
C29	216 ± 3	214 ± 3	168/192 ± 3	172/188 ± 5
C30	213 ± 8	210 ± 10	172/188 ± 7	173/187 ± 7
C37	229 ± 5	229 ± 4	169/191 ± 6	172/188 ± 8
U38	*204* ± 17	–	172/188 ± 8	172/188 ± 8
C39	*219* ± 6	*215* ± 6	169/191 ± 4	173/187 ± 7
U40	*219* ± 4	*216* ± 4	168/192 ± 2	168/192 ± 2
C41	*217* ± 11	*215* ± 11	172/188 ± 8	172/188 ± 8
G44	219 ± 4	216 ± 4	169/191 ± 2	170/190 ± 3
C45	214 ± 8	210 ± 8	173/187 ± 7	174/186 ± 6
Hexanucleotide loop				
U31	*223* ± 4	*223* ± 4	averaged (90–270°)	averaged (90–270°)
G32	*216* ± 4	*215* ± 4	averaged (90–270°)	averaged (90–270°)
A35	averaged *trans-gauche-*	averaged *trans-gauche-*	averaged (90–270°)	averaged (90–270°)
Others				
G26	slow conformational exchange	slow conformational exchange	slow conformational exchange	slow conformational exchange
G36	239 ± 3 or slow conformational exchange	239 ± 3 or slow conformational exchange	162/198 ± 1 or slow conformational exchange	164/196 ± 1 or slow conformational exchange

[a]β and ε torsion angles for the nucleotides of the HIV-2 TAR RNA listed in column 1. The ε angle $C4'_i$-$C3'_i$-$O3'_i$-P_{i+1} is referred to the nucleotide i+1. The values for ε are reported in italics when only the $^3J_{PiH3'i-1}$ is available. In this case the ε torsion angle that is closer to that expected for a standard A-form helix is given. Two possible values of β satisfy the experimental data, due to the lack of stereospecific assignment of the H5′/H5″ protons. Columns 2 and 4 report on the results of fitting the experimental intensities to Equation 2 with $^4J_{PiH4'i} = 0$ (three parameters fitting: I_0, $^3J_{PH3'}$, β); columns 3 and 5 report on the results of fitting the experimental intensities to Equation 2 with $0.1 \leq {}^4J_{PiH4'i} \leq 2.9$ Hz (four parameters fitting: I_0, $^3J_{PH3'}$, β, $^4J_{PiH4'i}$).

than for the HIV-2 TAR RNA, due to slower relaxation processes ($R_2^* \approx 11$ Hz) and consequently higher signal-to-noise ratio. The ε and β values found for the nucleotides in the stem region are in excellent agreement to what expected for an A-form helical geometry, further verifying the validity of the proposed method.

Simulations

The methodology presented here relies on the assumption that the relaxation term R_2^* can be measured with the sequence of Figure 1b. The assumption is justified when $(2\pi J_{PH})^2 \gg (R_P\text{-}R_{PH})^2$. This condition is evidently not fulfilled for the geminal H5′/H5″ protons, for which we estimated a longitudinal relaxation time T_1 of ∼100 ms for the 30mer HIV-2 TAR RNA ($\tau_c = 4.0$ ns, unpublished result). Moreover, cross-correlation effects among the protons can also affect

the accuracy of the J coupling values. To evaluate the influence of relaxation phenomena on the accuracy of the measured couplings, we simulated the behavior of the spin system P_i, $H3'_{i-1}$, $H5'_i$, $H5''_i$, assuming a standard A form helical geometry ($J_{PH3'} = 9.0$ Hz, $\beta = 168.0°$). The relaxation properties of the protons were described considering H-H dipolar relaxation contributions among all protons with inter-nuclear distance $d_{HH} < 4.0$ Å and for the phosphorus relaxation only the chemical shift anisotropy contribution was taken into account (Herzfeld et al., 1984). A global correlation time of 4.0 ns was used in the calculations. Both experiments of Figures 1a and 1b were simulated for the same experimental time course and the procedure described above was used to extract the J coupling and torsion angle values. The effective R_2^* rate extracted from the simulated experiments of Figure 1b was 1.1 Hz larger than the transversal relaxation rate R_2 of the phosphorus, as expected due to the contributions of the longitudinal relaxation of the protons ($R_{1,H3'} \approx 3$ Hz). The $J_{PH3'}$ scalar coupling and the angle β measured from the time dependence of the P-H3′ peak in the simulated PH-CT-COSY experiments differ by less than 1% from the theoretical value. This verifies the fulfillment of the condition $(R_P\text{-}R_{PH})^2 < (2\pi J_{PH})^2$ for the J-coupled P-H3′ spin system. If the P-H5′ and P-H5″ cross peak intensities were used to extract the desired $J_{PH3'}$ and β values, a larger deviation of the measured parameters from the theoretical one was observed. The least accurate results were obtained using the P-H5″ peak, for which $(R_P\text{-}R_{PH})^2 \approx (2\pi J_{PH})^2$; nevertheless, even in this case the extracted $J_{PH3'}$ coupling and β angle deviate from the theoretical values by only 5%.

In order to investigate further the effect of the proton longitudinal relaxation rate R_{1H} on the accuracy of the measured couplings, we simulated a two spin system P-H with $J_{PH} = 5.0$ Hz and $R_{1H} = 2.0$, 10.0 or 50.0 Hz. The transversal relaxation rate of the J-coupled phosphorus nucleus R_{2P} was equal to 21.4 Hz. The effective R_2^* values measured with the pulse sequence of Figure 1b are 21.6 Hz, 22.3 Hz and 23.4 Hz for a R_{1H} of 2.0, 10.0 and 50.0 Hz, respectively. The constant time T for the sequence of Figure 1a was varied in the simulations in steps of 10 ms ranging from 20 to 180 ms. The simulated data obtained with the PH-CT-COSY sequence after deconvolution of the relaxation dependence term are shown in Figure 6a. The data were fitted to the function of Equation 3, for the measurement of the J_{PH} coupling constant. For $R_{1H} = 2.0$ Hz (solid curve,

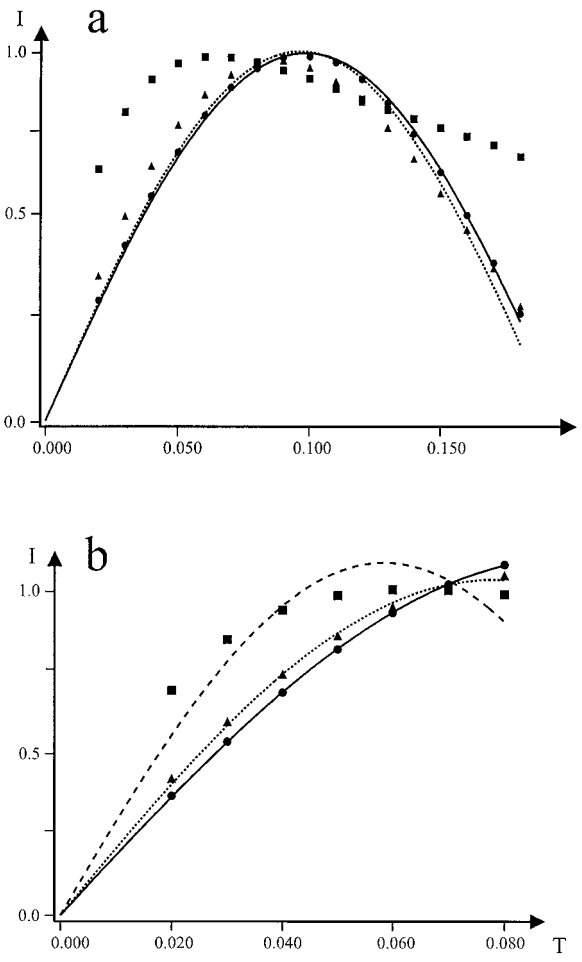

Figure 6. (a) Simulated peak intensities for the sequence of Figure 1a, after deconvolution of the relaxation term, for a two spin system AB, with $J_{AB} = 5.0$ Hz and $R_{1B} = 2.0$ Hz (solid dots), 10.0 Hz (solid triangles) and 50 Hz (solid squares). The R_2^* constants were derived from the sequence of Figure 1b, simulated for the three combinations of J_{AB} and R_{1B} described above. If the constant time T is varied between 20 and 180 ms, the data for the case where $J_{AB} = 5.0$ Hz and $R_{1B} = 50$ Hz cannot be satisfactorily fitted to the function of Equation 3 and no accurate J value can be extracted. The data represented by the solid triangles can be fitted to the function of Equation 3 and a J_{AB} of 5.19 Hz is extracted. This value deviates by 4% from the theoretical one ($J_{AB} = 5$ Hz). A J_{AB} of 5.08 Hz is measured from the data represented by the solid dots, that deviates by less than 2% from the theoretical one. (b) The same data as in panel (a) for T = 20–80 ms. A less accurate J_{AB} value is obtained if the constant time T is limited to 80 ms. The extracted coupling constant values are: $J_{AB} = 5.35$ Hz (solid dots), 6.39 Hz (solid triangles). The data for the combination $J_{AB} = 5.0$ Hz and $R_{1B} = 50$ Hz cannot be satisfactorily fitted to the function of Equation 3, as shown by the poor agreement of the dashed line with the solid squares data points.

solid dots), the quality of the fitting is excellent and the measured J_{PH} is 5.08 Hz. For $R_{1H} = 10.0$ Hz (dotted line, solid triangles), the quality of the fitting is acceptable and the measured J_{PH} is 5.19 Hz. For the case where $R_{1H} > 2\pi J_{PH}$ (solid squares) the data largely deviates from the function of Equation 3 and no J_{PH} value can be extracted. The accuracy of the measured J_{PH} improves when the sine function of Equation 3 is sampled for $T > 1/J$. However, in practice the transversal relaxation rate R_2 of the phosphorus for RNA molecules in the order of 10 kDa limits the maximum constant time T to 80–100 ms at 600 MHz. If one attempts to measure scalar couplings of the order of 5 Hz for a maximum constant time T of 80 ms (Figure 6b), a smaller accuracy of the measured value is to be expected (measured $J_{PH} = 5.35$ Hz for $R_{1H} = 2.0$ Hz; 6.39 Hz for $R_{1H} = 10.0$ Hz; 8.56 Hz for $R_{1H} = 50.0$ Hz). In this case the condition $R_{1H} \leq J$ needs to be verified, to ensure that the extracted J value is accurate within a 90% confidence.

Dipolar couplings

The experiment of Figure 1a was adapted to measure D_{PH} dipolar couplings between the phosphorus nucleus P_i and either the H6/H8 base protons of the same nucleotide or the H2′ sugar protons of the preceding nucleotide. To obtain selective coupling between the phosphorus and the desired protons, the π(H) pulse in the constant time T was substituted by a shaped pulse, selectively inverting either the H6/H8 base protons region (7.0–8.8 ppm) or the H2′ sugar protons region (4.0–5.0 ppm). Due to the extensive spectral overlap of the H2′, H3′, H4′, H5′ and H5″ sugar protons, selective coupling of the P nuclei to the H2′ protons can only be accomplished by usage of selectively deuterated nucleotides. In this case the P-H2′ dipolar couplings were measured for a RNA molecule consisting of d4-nucleotides, where the H3′, H4′, H5′ and H5″ protons had been substituted with deuterons (Tolbert and Williamson, 1996, 1997; Scott et al., 2001). Additionally, a homonuclear decoupling scheme was applied during the acquisition time, as previously described (Hennig et al., 2001), to eliminate the line broadening originating from H-H dipolar couplings. The experiments were performed for 1 mM HIV-2 TAR RNA aligned in a Pf1 filamentous bacteriphage solution (ASLA, Ltd., Riga, Latvia) of 44 mg/ml. The P-H_{base} correlation is shown in Figure 7.

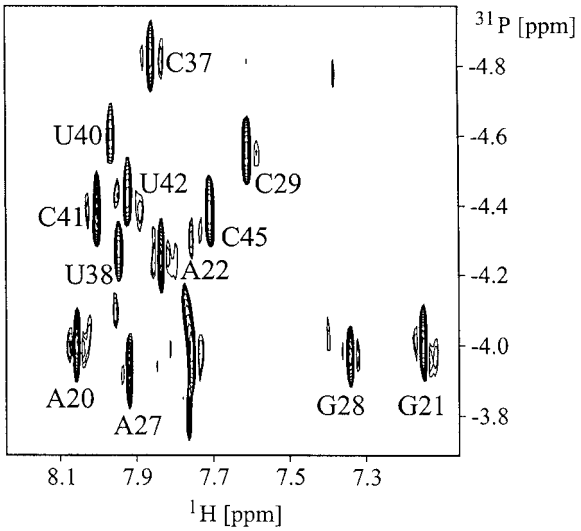

Figure 7. Two-dimensional P-H_{base} correlation recorded with the sequence of Figure 1a modified for the measurement of D_{PH} couplings. The π(H) hard pulse during the constant time delay T was substituted with a π(H) Q3 pulse of 2.4 ms. The proton carrier was at 7.65 ppm and the phosphorus carrier was at −3.65 ppm. HS homonuclear band selective time-shared adiabatic decoupling was applied in t_2. Adiabatic hyperbolic secant inversion pulses (Silver et al., 1984) of duration of 6.67 ms covering a bandwith of 1400 Hz were applied at 4.88 ppm with a duty cycle of 10%. Sixteen complex points were acquired for the phosphorus dimension. After mirror image linear prediction in the indirect dimension and zero-filling in both dimensions, the final matrix was $2048(\omega_2) \times 128(\omega_1)$ points. The constant time T was 40 ms. Spectra were processed and analyzed with FELIX 2000 (MSI, San Diego, U.S.A.). The P_i-$H_{base,i}$ peaks are identified according to the *i* nucleotide. The HIV-2 TAR RNA was aligned in a Pf1 filamentous bacteriophage solution of 44 mg/ml. The sample buffer contained 10 mM phosphate buffer, pH 6.4, 50 mM sodium chloride, and 0.1 mM EDTA in 500 µl of 99.9% D_2O.

Due to the large R_2^* of phosphorus, constant time delays T longer than ∼100 ms could not be used and a reliable quantification of the small D_{PH}s (< 5.0 Hz) was not possible (see the Simulations section). However, we can qualitatively map the intensity of the observed P-H peaks on the secondary structure of the HIV-2 TAR RNA (Figure 8). The one letter code corresponding to the nucleotide *i* in the RNA sequence is circled if a P_i-$H_{base,i}$ peak (Figure 8a) or a P_i-$H2'_{i-1}$ peak (Figure 8b) was observed in a P-H_{base} or a P-H2′ correlation. The gray scale in Figure 8 is directly proportional to the P-H peak intensity. The pattern of distribution of the $D_{PiH6/8,i}$ and of the $D_{PiH2'i-1}$ dipolar couplings is different and in general the absolute size of the two types of D_{PH}s is anticorrelated. This observation is consistent with the fact that the internuclear vectors sample different direc-

tions of the three-dimensional space. The non-uniform distribution of both the $D_{PiH6/8,i}$ and $D_{PiH2'i-1}$ couplings indicate that these dipolar couplings contain valuable structural information and that their values are not averaged by extensive internal motion. We are in the process of evaluating the impact of introducing qualitative D_{PH}-derived restraints in structure calculations.

Discussion

The PH-CT-COSY experiment allows the measurement of the three vicinal $^3J_{PH}$ scalar couplings related to the β and ε torsion angles in oligonucleotides by analyzing the time dependence of the P_i-$H3'_{i-1}$ cross peak. The proposed approach has considerable advantages with respect to the methods presented in the literature. The geminal H5′/H5″ protons are usually severely overlapped in RNAs, and for example, only 40% of the H5′/H5″ protons could be resolved for the HIV-2 TAR RNA in a C-H correlation. Moreover, prohibitively long constant time delays during which the H5′/H5″ magnetization is transverse, as required by J-HMBC and quantitative J correlation spectroscopy, are impracticable for large RNAs. Very efficient H-H dipolar relaxation mechanism and the presence of the large geminal $^2J_{HH}$ scalar coupling result in unfavorable line broadening of the H5′/H5″ resonances (Kaikkonen and Otting, 2001). In the method proposed here neither the overlap of the H5′/H5″ region nor the fast relaxation of the H5′/H5″ protons impede the measurement of the $^3J_{PH5'/H5''}$ couplings, as they are extracted by analyzing the time decay of the better behaved P-H3′ cross peak. The overlap of the $H3'_{i-1}$ proton with the $H5'_i$ proton and of H3′ protons belonging to different nucleotides can be efficiently solved by adding a ^{13}C editing step, as suggested in Figure 1c.

Interestingly, the quantitative analysis of the time dependence of the intensity of the P-H3′ cross peak reveals the presence of conformational averaging around the β torsion angle. This can be attributed to the simultaneous dependence of the intensity of this cross peak on both passive $^3J_{PH5'}$ and $^3J_{PH5''}$ couplings. If a sufficient signal-to-noise ratio can be obtained for the P-H3′ peak, different models of conformational averaging around the torsion angle β can be used to fit the time decay of the peak intensity. It is quite promising that the data for those nucleotides with degenerate H5′/H5″ protons could be accurately fitted with a model that assumes fast averaging around the β torsion angle yielding equal $^3J_{PH5'}$ and $^3J_{PH5''}$ couplings. For G33, where the H5′/H5″ protons have distinct but very similar chemical shifts, the model that assumes equal $^3J_{PH5'/H5''}$ couplings fails to successfully fit the data.

The PH-CT-COSY methodology does not require expensive ^{13}C labeling of the RNA and 58% of the $^3J_{PH}$ scalar couplings were successfully extracted for the unlabeled 30mer TAR-RNA. However, for a more complete analysis of the $^3J_{PH}$ couplings, a better separation of the H3′ protons is needed. This can be achieved by adding a ^{13}C editing step (Figure 1c). For a ^{13}C labeled molecule the H3′ T_1 relaxation times will significantly decrease, due to the additional efficient ^{13}C-^1H dipolar relaxation mechanism. Nevertheless, theoretical simulations show that the coupling constants extracted with the PH-CT-COSY methodology are accurate within 5% of the real value even in the limit where $R_1 = 2{*}J_{PH}$. This degree of accuracy represent the optimum achievable in measuring coupling constants for biomolecules independently of the methodology, due to systematic errors introduced by differential relaxation effects (Harbison, 1993; Norwood, 1993).

The phosphodiester backbone conformation is poorly defined in NMR structures calculated by NOE restraints only. In the structure calculation of the HIV-1 TAR RNA (Aboul-ela et al., 1996) semi-quantitative restraints on the β and ε torsion angles have been introduced based on the observation of a peak in a PHCH correlation spectrum, while no restraints on β and ε have been used for structure calculation of the HIV-2 TAR RNA bound to argininamide (Brodsky et al., 1997).* For the oligonucleotides in standard A-form helical region (17, 20, 29 and 37–45 in Table 2), we find average β and ε angles of 170/190° and 217°, respectively, that compare well with the average values for the corresponding nucleotides in the HIV-1 TAR RNA structure ($\beta_{av} = 188° \pm 34°$ and $\varepsilon_{av} = 225° \pm 18°$) by Aboul-ela et al. and in the HIV-2 TAR RNA/argininamide structure by Brodsky et al. ($\beta_{av} = 188° \pm 22°$ and $\varepsilon_{av} = 192° \pm 35°$). The distribution of values for the ε torsion angle of residues in helical regions is very narrow. Conformational averaging around the β and possibly ε torsion angles is found in the present study for most of the nucleotides located in the loop (Table 1).

Of special interest is the value for the ε torsion angle $C4'_{25}$-$C3'_{25}$-$O3'_{25}$-P_{26}. Upon binding of argini-

*The HIV-1 and HIV-2 TAR RNA are virtually identical, except for the bulge region, that comprises three and two nucleotides in the HIV-1 and HIV-2 TAR RNA, respectively

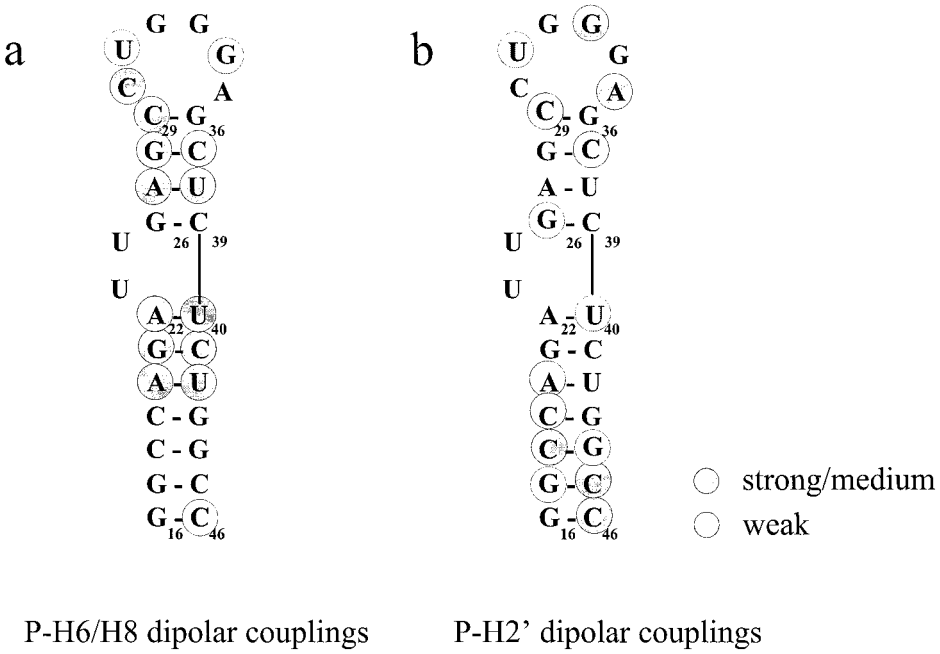

Figure 8. Map of the intensity of the P_i-$H6_i$/$H8_i$ (a) and P_i-$H2'_{i-1}$ peaks (b) on the secondary structure of the HIV-2 TAR RNA. Each P-H connectivity has been attributed to the nucleotide *i*. The peaks were observed in P-H_{base} and P-H2′ correlations recorded with the pulse sequence of Figure 1a, modified to observe dipolar couplings, as described in the caption to Figure 7. Dark gray circles correspond to strong peaks, light gray circles to peaks of medium/weak intensity. The absence of a circle indicates that no P-H peak mediated by residual dipolar couplings could be observed.

namide or cognate peptides the TAR RNA undergoes major conformational changes in the bulge region. The base triple U38-A27 · U23 is formed and the nucleotide U25 is projected into solution. The $C4'_{25}$-$C3'_{25}$-$O3'_{25}$-P_{26} torsion angle is 221° ± 26° in the HIV-1 TAR RNA structure by Aboul-ela et al., similar to the value of 248° ± 23° found for the HIV-2 TAR RNA/argininamide structure by Brodsky et al. However, our coupling values suggest the presence of slow conformational averaging for both the ε and β torsion angles. Aboul-ela et al. conclude from the lack of NOE constraints involving U25 that this nucleotide might be disordered in the HIV-1 TAR RNA (Aboul-ela et al., 1996). The peculiar behavior of G26 demonstrates the importance of obtaining torsion angles restraints in non-helical regions. Structural perturbations due to the lack of complete base complementarity of the intramolecular duplex strands are quite common in RNA and often constitute the site of intermolecular interactions. It is essential to provide experimental tools to describe the non-helical structure that RNA assumes to interact with other molecules and thus exert its biological function.

The methodology was originally designed to measure D_{PH} dipolar couplings between the phosphorus nucleus and the H6/H8 base protons (Hennig et al., 2001) for partially oriented HIV-2 TAR RNA in a Pf1 bacteriophage solution. Unfortunately, these couplings were found to be smaller than 5 Hz while the longitudinal relaxation rate R_1 for the H6/H8 base protons is estimated to be approximately 10 Hz due to the close proximity of the H2′ proton of the preceding nucleotide. With the effective R_2^* relaxation rate of the phosphorus nuclei being in the order of 30 Hz, the maximum constant time delay T applicable was 100 ms. With these limitations the couplings constants can be measured with only 75% accuracy (see the Simulations section). More accurate values of the couplings could be obtained by a thorough comparison of the experimental intensity decay with simulated data, taking both R_{2P} and R_{1H} into account. Alternatively, the experiments can be performed at lower fields, where the CSA contribution to the phosphorus relaxation is reduced. The PH-CT-COSY method can be easily employed to measure D_{PH} dipolar couplings in small RNA molecules, where, due to the slower R_{2P} and R_{1H}, longer constant time delays are

feasible. It should be noted that the accurate measurement of small couplings between rapidly relaxing nuclei is inherently difficult. This is true also for spin-echo difference experiments, where the coupling constant is extracted from differences in cross peak I_A and I_B intensities according to the function $J = \cos^{-1}(I_A/I_B)/2\pi T$ (Vuister et al., 1998). In this case the constant time delay T must be sufficiently long to assure a significant deviation from the condition $\pi JT = 0$ and $\cos(\pi JT) = 1$ with respect to the signal-to-noise ratio. This requirement is increasingly difficult to meet for fast relaxing coherences. Moreover, longer constant time delays T are associated with increasing differential relaxation effects.

Conclusions

We have presented a new method to measure J_{PH} scalar couplings related to the phosphodiester backbone torsion angles β and ε in nucleic acids. The advantage of the proposed method lies in the possibility of extracting the vicinal $^3J_{PH3'}$ scalar coupling and the β torsion angle by the quantitative analysis of the intensity decay of the P_i-$H3'_{i-1}$ cross peak. This allowed us to obtain accurate values of the β torsion angle even in the presence of severely overlapped H5′/H5″ proton resonances.

The technique has been applied to the unlabeled 30mer HIV-2 TAR RNA allowing for a quantitative analysis of 58% of the nucleotides. We were able to distinguish between different analytical models for individual nucleotides reflecting specific conformational averaging processes. If necessary, the resolution can be improved by adding a ^{13}C editing step. The new method is suitable for RNAs molecules as large as 10–15 kDa. Additionally, the PH-CT-COSY approach allows the measurement of P-H dipolar couplings in small nucleic acids. Detailed experimental and theoretical results, considering the involved relaxation mechanisms of ribose protons and phosphorus nuclei, are presented that should provide guidelines for further investigations of the phosphodiester backbone conformations and interactions involving ^{31}P nuclei by NMR methods.

Acknowledgements

This work was supported by a grant from the National Institutes of Health to J.R.W. (GM-56552) and by the Skaggs Institute for Chemical Biology. M.H. acknowledges support from the Human Frontier Science Program. We thank Jeff Chao for preparing the 14mer GAAG tetraloop RNA and Lincoln G. Scott for providing specifically deuterated NTPs.

References

Aboul-ela, F., Karn, J. and Varani, G. (1996) *Nucl. Acids Res.*, **24**, 3974–3981.

Bevington, P.R. and Robinson D.K. (1992) *Data Reduction and Error Analysis for the Physical Sciences*, WCB/McGraw-Hill, U.S.A.

Billeter, M., Neri, D., Otting, G., Qian, Y.Q. and Wüthrich, K. (1992) *J. Biomol. NMR*, **2**, 257–274.

Brodsky, A.S. and Williamson, J.R. (1997) *J. Mol. Biol.* **267**, 624–639.

Cavanagh, J. Fairbrother, W.J., Palmer, A.G. III and Skelton, N.J. (1996) *Protein NMR Spectroscopy: Principles and Practice*, Academic Press, San Diego, CA, pp. 279–281.

Clore, G.M., Murphy, E.C., Gronenborn, A.M. and Bax, A. (1998) *J. Magn. Reson.*, **134**, 164–167.

Gotfredsen, C.H., Meissner, A., Duus, J.Ø. and Sørensen, O.W. (2000) *Magn. Reson. Chem.*, **38**, 692–695 .

Harbison, G.S. (1993) *J. Am. Chem. Soc.*, **115**, 3026–3027.

Hennig, M. Carlomagno, T. and Williamson, J.R. (2001) *J. Am. Chem. Soc.*, **123**, 3395–3396.

Hines, J.V., Varani, G., Landry, S.M. and Tinoco, Jr., I. (1993) *J. Am. Chem. Soc.*, **115**, 11002–11003.

Herzfeld, J., Griffin, R.G. and Haberkorn, R.A. (1984) *Biochemistry*, **17**, 2711–27184.

Hu, W., Bouaziz, S., Skripkin, E. and Kettani, A. (1999) *J. Magn. Reson.*, **139**, 181–185.

Kaikkonen, A. and Otting, G. (2001) *J. Biomol. NMR*, **19**, 273–277.

Lankhorst, P.P., Haasnoot, C.A., Erkelens, C. and Altona, C. (1984) *J. Biomol. Struct. Dyn.*, **1**, 1387–1405.

Legault, P., Jucker, F.M. and Parti, A. (1995) *FEBS Lett.* **362**, 156–160.

Long, K.S. and Crothers, D.M. (1999) *Biochemistry*, **38**, 10059–10069.

Marino, J.P., Schwalbe, H., Glaser, S.J. and Griesienger, C. (1996) *J. Am. Chem. Soc.*, **118**, 4388–4395.

Murthy, V.L., Srinivasan, R., Draper, D.E. and Rose, G.D. (1999) *J. Mol. Biol.*, **291**, 313–327.

Norwood, T.J. (1993) *J. Magn. Reson.*, **A104**, 106.

Plavec, J. and Chattopadhyaya, J. (1995) *Tetrahedron Lett.*, **36**, 1949–1952.

Puglisi, J.D., Tan, R., Calnan, B.J., Frankel, A.D. and Williamson, J.R. (1992) *Science*, **257**, 76–80.

Richter, C., Reif, B., Worner, K., Quant, S., Marino, J.P., Engels, J.W., Griesienger, C. and Schwalbe, H. (1998) *J. Biomol. NMR*, **12**, 223–230.

Saenger, W. (1984) *Principles of Nucleic Acid Structure*, Springer-Verlag, New York, NY.

Schwalbe, H., Marino, J. P., King, G.C., Wechselberger, R., Bermel, W. and Griesienger C., (1994) *J. Biomol. NMR*, **4**, 631–644.

Schwalbe, H., Samstag, W., Engels, J.W., Bermel, W. and Griesienger, C. (1993) *J. Biomol. NMR*, **3**, 479–486.

Scott, L.G., Tolbert, T.J. and Williamson, J.R. (2000) *Meth. Enzymol.*, **317**, 18–38.

Silver, M.S., Joseph, R.I. and Hoult, D.I. (1984) *J. Magn. Reson.*, **59**, 347.
Sklenar, V. and Bax, A. (1987) *J. Am. Chem. Soc.*, **109**, 7525–7526.
Sklenar, V., Miyashiro, H., Zon, G., Miles, H.T. and Bax, A. (1986) *FEBS Lett.*, **208**, 94–98.
Szyperski, T., Ono, A., Fernandez, C., Iwai, H., Tate, S., Wüthrich, K. and Kainosho, M. (1997) *J. Am. Chem. Soc.*, **119**, 9901–9902.
Tao, J. and Frankel, A.D. (1992) *Proc. Natl. Acad. Sci. USA*, **89**, 2723–2726.
Tao, J. and Frankel, A.D. (1993) *Proc. Natl. Acad. Sci. USA*, **90**, 1571–1575.
Tian, F., Bolon, P.J. and Prestegard, J.H. (1999) *J. Am. Chem. Soc.*, **121**, 7712–7713.
Tolbert, T.J. and Williamson, J.R. (1996) *J. Am. Chem. Soc.*, **118**, 7929–7940.
Tolbert, T.J. and Williamson, J.R. (1997) *J. Am. Chem. Soc.*, **119**, 12100–12108.
Varani, G., Aboul-ela, F., Allain, F. and Gubser, C.C. (1995) *J. Biomol. NMR*, **5**, 315–320.
Vuister, G. W., Tessari, M., Karimi-Nejad, Y. and Whitehead, B. (1998) *Modern Techniques in Protein NMR*, Kluwer Academic/ Plenum Publishers, New York, pp. 204–212.
Wijmenga, S.S. and van Buuren, B.N.M. (1998) *Progr. Nucl. Magn. Reson. Spectrosc.*, **32**, 287–387.
Wu, Z. and Bax, A. (2001) *J. Magn. Reson.*, **151**, 242–252.
Zacharias, M. and Hagerman, P.J. (1995) *Proc. Natl. Acad. Sci. USA*, **92**, 6052–6056.